THE JOURNAL OF PHYSICAL CHEMISTRY C

Article

Cite This: J. Phys. Chem. C 2019, 123, 17510−17520

pubs.acs.org/JPCC

Nucleation Mechanisms of Self-Assembled Physisorbed Monolayers on Graphite

Tomasz K. Piskorz,[†] Cristian Gobbo,[†] Siewert J. Marrink,[§] Steven De Feyter,[‡] Alex H. de Vries,[§] and Jan H. van Esch*[,†]

[†]Advanced Soft Matter, Chemical Engineering, Delft University of Technology, van der Maasweg 9, 2629 HZ Delft, The Netherlands

[‡]Department of Chemistry, KU Leuven, Celestijnenlaan 200F, 3001 Leuven, Belgium

[§]Groningen Biomolecular Sciences and Biotechnology Institute and Zernike Institute for Advanced Materials, University of Groningen, Nijenborgh 4, 9747 AG Groningen, The Netherlands

Supporting Information

ABSTRACT: Coarse-grained molecular dynamics simulations are employed to obtain a detailed view of the formation of long-range ordered lamellar structures of physisorbed self-assembling long functionalized alkanes on graphite. During the self-assembly, two processes take place: Langmuir preferential adsorption and rearrangement on the surface. The rearrangement starts with nucleation, in which molecules create an ordered domain. The nucleation mechanism is temperature dependent. At lower temperature independent, small and stable nuclei seed the emergence of long-range ordered domains. In contrast, at a higher temperature, molecules adsorb on the surface, and only when a certain level of surface coverage by the adsorbent is reached, the whole structure undergoes a transition from a liquid-like structure to an ordered structure. After this step, relatively slow corrections of the structure take place by Ostwald ripening.

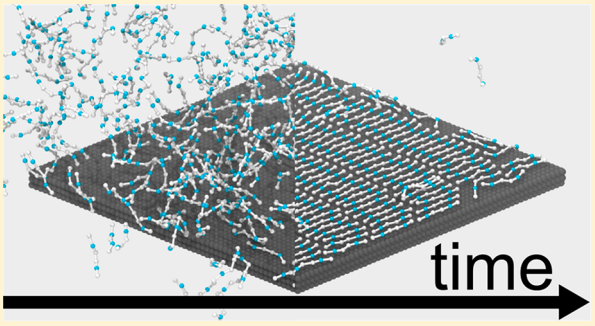

INTRODUCTION

Self-assembly on a surface has emerged as a promising method to fabricate two-dimensional structures on the nanoscale. In recent years, considerable improvement has been achieved in this field as evidenced by the growing number and complexity of obtained structures.[1] Here, we focus on the formation of physisorbed self-assembled monolayers (often referred to as self-assembled molecular networks, SAMNs), which could be an alternative approach to obtaining small two-dimensional devices on the single-molecular scale.[2−5] Such monolayers could have application in industry, e.g., in nanoelectronics, in which conventional methods have almost reached their limits.[6] Despite many efforts, it is still challenging to predict the final assembled morphology from the molecular structure of the adsorbent. Therefore, understanding underlying mechanisms of self-assembly is crucial to tackle this problem.[7]

There are many studies devoted to self-assembled molecular networks and many different techniques are used, of which scanning tunneling microscopy (STM) has given the most significant insights.[1,8] STM allows observing the actual distribution of atoms on an atomistic scale. It does not require periodic structure, and therefore, it can observe defects, grain boundaries, and different polymorphs on the surface. Besides studies of the final assembly, STM has been used to study thermodynamic aspects of the mechanism of formation of SAMNs. A well-accepted model to describe the formation of SAMNs is based on nucleation and growth.[9] Matsuda et al.[10−15] have proposed that similar formation mechanisms as in supramolecular polymerization are present for SAMNs: the isodesmic mechanism, in which molecules as they adsorb to the surface join ordered domains, and the cooperative mechanism, in which a certain concentration of molecules has to be present on the surface before ordered domains can be formed. Depending on the chemical nature of the molecular building block the formation of the assembly can follow one of these paths.[11] However, the kinetics of processes involved in the mechanisms, such as nucleation and growth are too fast to be observed by STM,[7] and the mechanisms that operate often cannot be determined with certainty. To our knowledge, experimental studies at the liquid−solid interface show only how already formed lamellar structures exchange adsorbent molecules with those in solution and rearrange to heal defects.[16] One way to address this problem is to use computational methods that are suitable to study dynamic processes at the molecular length scale and at high time-resolution. Several simulation studies of self-assembly on a

Received: February 7, 2019
Revised: May 10, 2019
Published: May 10, 2019

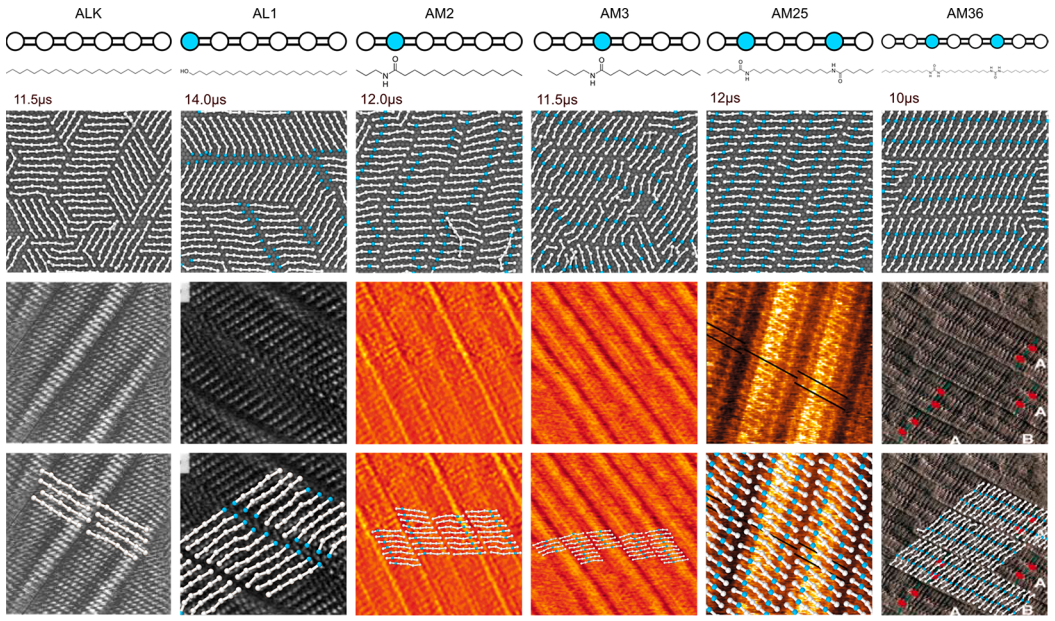

Figure 1. Martini model of long-chain functionalized alkanes and final structures of assemblies with comparison to experimental results. The top row shows the Martini models used for the adsorbent molecules labeled ALK, AL1, AM2, AM3, AM25, and AM36. White circles denote alkyl-type beads (C1S and C1E); blue beads denote polar beads (P1). Molecular structures at atomistic resolution are shown below for molecules the coarse-grained model may represent. The second row shows the final self-assembled structures of these molecules on a graphite surface obtained from the simulations and the simulation time at which they were obtained. The third row shows STM/AFM images of the molecules the coarse-grained model may represent (see main text). The bottom row shows experimental results of self-assembled structures with fragments of the simulated structures superimposed. For the molecules represented by the structures of ALK, AL1, and AM25, structures were available in the literature for the molecules as suggested by the standard mapping of Martini.[35,67,68] For AM36, AM2, and AM3, we compare with results for the most similar molecules that we found in the literature.[32,69] Although lamellar structures for molecules represented by AM36 with amides as the polar groups were reported in the literature (which are more distorted in comparison with AM25, which we also observe), the structure was not shown.[68] Therefore, here we present results for molecule represented by AM36 with urea groups instead of amide (the urea group prevents molecules from tilting, therefore a different angle for simulation and experiment can be observed). Figure adapted with permission from Askadskaya et al.[67] and Buchholz et al.[35] Copyrights 1992, the American Physical Society, and John Wiley and Sons.

surface have been reported. Most of them are based on two-dimensional (2D) Monte Carlo (MC) and molecular dynamics (MD) simulations[17−24] and study rearrangement of the molecules on the surface. Also the complete process, including adsorption and rearrangement on a surface, was studied for surfactants on a graphite flake,[25−28] however long-range ordered structure formation was not the subject of those studies.

In this paper, we applied coarse-grained molecular dynamics simulations to give insights into the complete process of self-assembly of SAMNs on graphite starting from adsorbent molecules in solution and ending with the ordered assembly on the graphite surface. As archetypical molecular layers, we selected the widely studied lamellar assemblies of long-chain alkanes and alkane derivatives on highly oriented pyrolytic graphite (HOPG).[29−32] In these assemblies, linear molecules in solution adsorb onto a substrate and adopt a straight-chain conformation on the surface, giving rise to parallel lamellae, as has been studied in detail by, e.g., STM.[30] Due to the weak forces involved, these structures display high conformational freedom, and moreover, the functionalization of alkanes resulted in observation of different arrangements (see Figure 1), allowing the investigation of chemical structure differences on monolayer formation. The model described here can predict final structures of the assembly and gives insights into the dynamics of the self-assembly processes, on a time scale that is not yet accessible by other techniques.

RESULTS AND DISCUSSION

The recently developed coarse-grained (CG) Martini model for functionalized long-chain alkanes adsorbing onto a graphite surface[33] was used to study the formation and structure of domains of six compounds that differ in substitution pattern and length (Figure 1). In the first part, we report the final structures formed on the microsecond simulation time scale and compare them with experimental results. Next, we focus on the mechanism by which these structures are formed, singling out the system (AM25) that forms the structure of highest quality in terms of long-range ordering and domain size.

Adsorbents Form Lamellae with Polar Substituents Determining Packing Efficiency. Figure 1 shows a schematic representation of the Martini model of the six adsorbent molecules studied, the final structures of the six systems obtained after at least 10 μs at 298 K, together with experimentally determined STM/AFM images of representative molecules, and a superposition of the CG structure on the experimental images. All of the adsorbent molecules form lamellar structures. The quality of the structures in terms of alignment of molecules increases with the number of polar substituent groups: it is strongest for molecules with two polar groups (AM25, AM36), less strong for molecules with one polar group (AL1, AM2, AM3), and least strong for the apolar molecules (ALK). This tendency agrees with the experimental results, in which amide groups impose strong directionality in assemblies.[34] Molecules in the lamellae tend to align with the

DOI: 10.1021/acs.jpcc.9b01234
J. Phys. Chem. C 2019, 123, 17510−17520

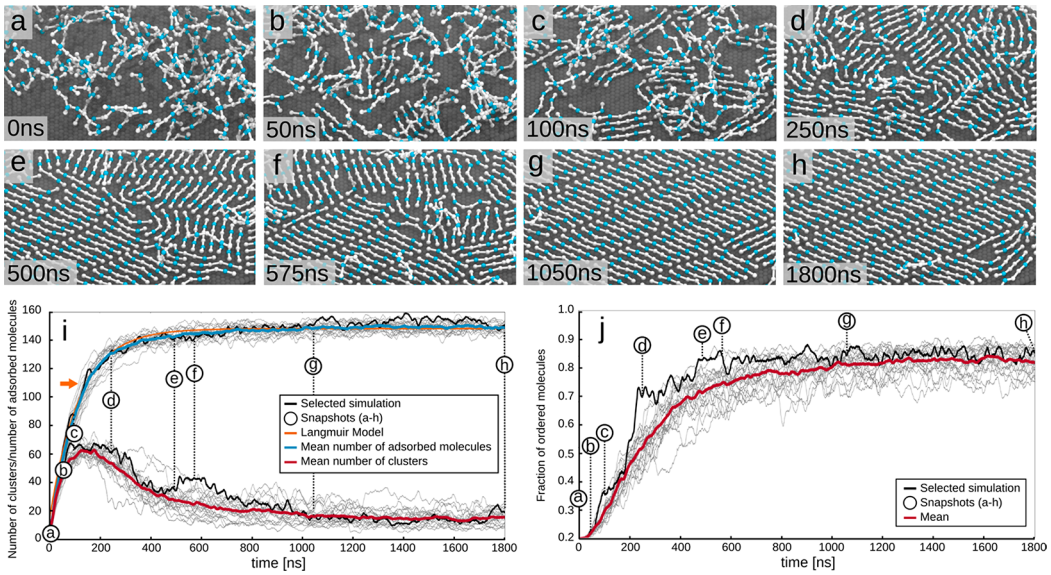

Figure 2. Snapshots from a representative simulation of AM25 at 298 K: (a, b) adsorption phase, (c−g) lamellar growth phase, and (h) structure after 1.8 μs of simulation. Solvent (phenyloctane) is not shown for clarity. The process of self-assembly on the surface can be described by monitoring the number of adsorbed molecules on the surface and the number of clusters (i), as well as the fraction of ordered molecules (j). In parts i and j, gray lines indicate results for 10 independent runs (i.e., 20 measurements: for every simulation there are two surfaces on which self-assembly process takes place) at 298 K, the thick black line results for an example trajectory (black dots correspond to snapshots a−g). In part i, the orange arrow indicates 70% surface coverage. The mean of the number of adsorbed clusters is shown as the thick blue line, and the mean of the number of clusters is shown as the thick red line. A fit of the mean number of adsorbed molecules to the Langmuir absorption rate law is shown as the thick orange line. In part j, the average fraction of ordered molecules is shown as a thick red line.

underlying graphite structure, of which the Martini beads are hexagonally packed, leading to three equivalent orientations. The main axis of the molecules aligns with a basal line of the graphite structure. Therefore, almost all adsorbed molecules are parallel or rotated by multiples of 60 deg with respect to each other (further quantification is given in the Supporting Information). Functionalized alkanes (i.e., AL1, AM2, AM3, and AM25) form assemblies which well reproduce experimental results. An exception is the long-chain alkane (ALK) for which molecules in simulation are also oriented with respect to each other in multiples of 60 deg, whereas in the experiment they form lamellae whose axis is perpendicular to the molecular vector. This shows a limitation of our model as a result of coarse-graining; understanding this limitation may enable development of a CG model that reflects the long-chain alkane packing (see Supporting Information for figures).

In the simulations, molecules with two symmetrically placed polar groups, AM25 and AM36, formed lamellae of the best quality in terms of alignment of the molecules and the size of the domains, at least on the time scale of the simulations. The quality of all final structures is further assessed in the Supporting Information. The excellent alignment of molecules with two symmetrically placed polar groups can also be seen in experimentally determined structures (Figure 1). Molecules with one polar bead, AL1, AM2, and AM3, due to their asymmetry, can orient in two distinct directions inside lamella, i.e., parallel and antiparallel. AL1 and AM2 neighboring molecules are predominantly parallel, driven by the favorable polar−polar and apolar−apolar interactions. Moreover, neighboring AL1 lamellae tend to face each other with their polar groups, and their final assembly features many defects, in which lamellae show kinks or are oriented by 120 deg with respect to each other. The abundance of these defects agrees with experimental results for long-chain alcohols,[35] and it is further shown in the Supporting Information. Comparing AM3 and AM2 assemblies, the lamellae of AM3 can be seen to be more disordered than those of AM2; see Figure 1. Two neighboring molecules within these lamellae can adopt a number of conformations, characterized by being parallel or antiparallel on the one hand and showing an offset on the other hand. The minimum offset in our model is half a bead in perfectly aligned lamellae (this leads to domain boundaries that are oriented at multiples of 60 deg). For both AM2 and AM3, the parallel−minimum offset conformation is the most frequent. In this conformation, the polar beads are next to each other and multiple lamellae can be stacked parallel to each other without defects or domain boundaries. A common relatively small defect is a so-called twin boundary, in which the offset changes from positive to negative. This results in a kink in the lamella. Another twin boundary with a negative to positive offset further down the lamella then causes a zigzag appearance; these types of structures have been reported for long-chain molecules.[36] This is a relatively cheap defect as long as parallel lamellae all follow the same zigzag pattern. Minimum offset but antiparallel conformations are costly: the polar beads are no longer neighbors, and the arrangements breaks multiple relatively favorable polar−polar and nonpolar−nonpolar interactions in return for relatively unfavorable polar−nonpolar bead interactions. The difference between AM2 and AM3 is that an offset of one bead (in the right direction of course) can restore the polar−polar and nonpolar−nonpolar interactions for the AM3 molecule but not for the AM2 molecule. The larger offset causes some misalignment between neighboring lamellae, but it is apparently not prohibitively costly. AM2 would need an offset of two beads to restore favorable polar−polar and nonpolar−nonpolar interactions, which apparently leads to such a severe

DOI: 10.1021/acs.jpcc.9b01234
J. Phys. Chem. C 2019, 123, 17510−17520

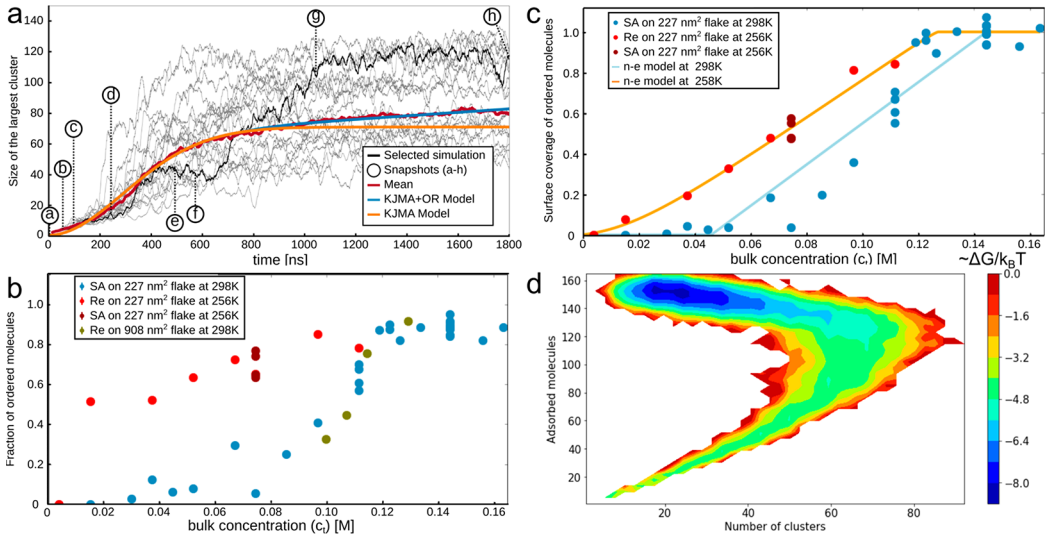

Figure 3. Size of the largest cluster as a function of time, fraction of ordered molecules as a function of concentration, and fraction of surface coverage of ordered molecules as a function of concentration, at different temperatures. (a) Size of largest cluster as a function of time. Results from 10 independent simulations at 298 K are shown as thin gray lines. The mean value from the simulations is shown as a thick red line. A fit of the mean value to the KJMA function with correction of Ostwald ripening (KMJA + OR, see text) is shown as a thick blue line. For comparison, a fit to the KJMA function without Ostwald ripening (KJMA) is also shown (thick orange line). (b) Fraction of ordered molecules as a function of bulk (i.e., total) concentration of adsorbent molecules in the system. Results are shown for two different graphite flake sizes and two different temperatures. At 258 K the ordering of the adsorbent molecules is higher than at 298 K at the lower bulk concentrations. At higher temperature, a relatively high concentration is required to obtain an ordered structure. (c) Fraction of surface covered by ordered molecules as a function of adsorbent bulk concentration. A fit of the nucleation-elongation model (n-e model) is shown as a thick light blue line at 298 K (fitted values: $\sigma = 6 \times 10^{-3}$, $K_e = 19\ M^{-1}$, and $\alpha = 0.091$ M) and as a thick orange line at 258 K (α is assumed to be the same as for 298 K (0.091 M); fitted values: $\sigma = 4 \times 10^{-6}$, $K_e = 33\ M^{-1}$) . For parts b and c, results are presented for the final frames of simulations of self-assembly (SA) from randomly distributed molecules in solvent or for a simulation of the rearrangement (Re) of adsorbed molecules that were already on the surface. Simulations were performed on graphite flakes with sizes of 227 nm^2 and 908 nm^2. (d) Free energy landscape obtained from distribution of states using metrics of number of adsorbed molecules and number of clusters. The color scale reflects the free energy proportional to the negative logarithm of the probability. For projections with the fraction of ordered molecules, see Supporting Information.

packing defect that it is only seen near the edges of the ordered assemblies.

In closing this section, it should be noted that coarse-graining of the system allows extending simulations to microsecond scale, but it is still several orders of magnitude shorter than the experimental scale (minutes). Furthermore, in coarse-graining, some details of the chemical structure are lost, and a comparison to the experimental systems can only be interpreted semiquantitatively. In that context, it should also be noted that we do not have a close experimental match for AM36 model to compare with (the image on Figure 1 shows a bisurea-functionalized molecule—the closest molecule that we found in the literature to AM36 which represents a bisamide molecule).

Self-Assembly Mechanism Depends on Temperature. Having shown that the Martini model is capable of yielding well-ordered lamellar structures of adsorbent molecules on graphite, the model is used to study the mechanism by which such structures are formed during the self-assembly process. We observed two processes occurring simultaneously throughout self-assembly: adsorption of long-chained molecules to and rearrangement of these molecules on the surface. In the latter process we could distinguish two phases: first a nucleation phase, in which an initial ordered structure is created, followed by an Ostwald ripening phase,[37−39] where the final ordered structure emerges. We also observed that depending on the temperature, the mechanism of nucleation changes. At higher temperatures (in the simulations that is 298 K) the adsorbed molecules initially form a liquid-like phase, which changes to the well-ordered structure at higher surface coverage. In contrast, at lower temperatures (258 K), adsorbed molecules immediately associate with each other creating semiordered clusters, which grow and eventually cover the graphite surface. To study the self-assembly process in more detail, we focused on AM25, which yields the highest quality long-range ordered final structure on the simulation time scale.

Cooperative Nucleation Mechanism at High Temperatures. At higher temperatures, AM25 molecules adsorb on the graphite surface forming a liquid-like phase, which after a while transforms to an ordered aligned structure. Parts a−h of Figure 2 show representative snapshots of this process (for the other molecules see Supporting Information). Starting from a random solution (Figure 2a), the molecules rapidly adsorb onto the surface, displacing the solvent phenyloctane (Figure 2, parts b and c). They form highly dynamic clusters with parallel oriented molecules (Figure 2, parts c and d), and diffuse on the surface as individuals and as clusters. The formed structure resembles a two-dimensional liquid and stays in this phase until no more molecules can adsorb on the surface (approximately 70% of surface coverage) unless reorganization occurs (Figure 2, parts e and f). When 90% of the surface is covered by adsorbent molecules, large lamellar domains can be seen (Figure 2f), which further rearrange into relatively large ordered structures (Figure 2g). After this stage, the assembly undergoes the slow process of Ostwald ripening: large clusters grow at the expense of small clusters, leading to a single domain that covers almost the entire graphite flake (Figure 2h). Most of the final structure is stable and just a

DOI: 10.1021/acs.jpcc.9b01234
J. Phys. Chem. C 2019, 123, 17510−17520

small fraction, on the edges of the flake, remains dynamic. On much longer time-scales, remaining defects heal; the mechanisms of the healing process are the subject of a recent study[40] and are not discussed here.

The self-assembly process is stochastic in nature—it is difficult to create a clear image of the process from a single trajectory, but after several independent self-assembly simulations, clear patterns characterizing the mechanism can be observed. The first 1.8 μs of 10 runs were analyzed by monitoring, as a function of time, the number of adsorbed molecules, the number of clusters, the fraction of ordered molecules, the surface coverage of ordered molecules, and the area of the largest cluster. A detailed description of the metrics can be found in the Supporting Information, but briefly, a cluster is defined by a combination of distance and orientation criteria between neighboring adsorbent molecules which are designed to detect groups of molecules that form a lamellar structure. Results of selected metrics for 10 independent simulations are shown in parts i and j of Figure 2 as thin gray lines, together with the average metrics in thicker lines, and they provide a clear picture on how surface coverage develops over time. We observed that the rate of adsorption follows the simple Langmuir growth law:[41,42] the rate of adsorption is proportional to the number of free spaces on the surface (Figure 2i, orange line). Thus, the number of adsorbed molecules can be expressed as a function of time by the relation

$$n_{ads}(t) = n_{\max}(1 - e^{-k_a t}) \tag{1}$$

where k_a is the adsorption rate and n_{max} is the maximal number of adsorbed molecules. In the beginning, adsorbed molecules do not create clusters: the number of adsorbed molecules (Figure 2i, blue line) is almost the same as the number of clusters (Figure 2, red line); i.e., nearby molecules are not identified as forming well-defined lamellae and single free molecules are present on the surface. After 50−100 ns, there is not enough space to adsorb new free molecules, which leads to rearrangement of adsorbed molecules, resulting in the appearance of larger clusters. After the initial adsorption phase, the number of clusters reaches a maximum and from this point on, the number of clusters steadily decreases and the structures rearrange to lamellae with longer-ranged order (Figure 2i).

The growth of long-range ordered structure can be described by the Kolmogorov−Johnson−Mehl−Avrami (KJMA) law:[38]

$$A(t) = A_{\lim}(1 - \exp[-(kt)^n]) \tag{2}$$

Here $A(t)$ denotes the size of the structure of interest at time t, A_{lim} is the final size of the cluster, and k and n are constants describing the rate of growth. The simplicity of the KJMA law has led to successful application in many phase transformation processes.[38] In most applications, all of the organized structure is monitored; due to the relatively small size of our surface, we were limited to measuring the size of the largest cluster instead. Figure 3a shows the best fit (orange line; fit parameters are given in the Supporting Information) of the size of the largest cluster (averaged over 10 independent runs, red line) to the KJMA law. Although the KJMA law perfectly describes the first stages of growth of the largest cluster, it fails to describe later stages of cluster growth in our simulations. In our simulations, the size of largest cluster does not stabilize, but it slowly continues to grow. This continuous growth is caused by Ostwald ripening (OR); large clusters are growing at the expense of small ones. The correction for this phenomenon can be expressed by an additional term in the KJMA function:[38,43]

$$A(t) = A_{\lim}(1 - \exp[-(kt)^n]) + \left(\frac{t - \tau_{OR}}{1 + \exp[-2\omega(t - \tau_{OR})]}\right)k_{OR} \tag{3}$$

Here k_{OR} describes the rate of Ostwald ripening and τ_{OR} describes the beginning of this process. The expression $\exp[-2\omega(t - \tau_{OR})]$ is a switching-on function (for $t \ll \tau_{OR}$ the Ostwald ripening part is absent) and the ω parameter describes the smoothness of the switching (width of the turning-on period). The KJMA + OR function as observed from our multiple independent simulations describes the mean value of the size of the largest cluster as a function of time well, and the best fit is shown in Figure 3a as the blue line. However, the fitted rates of Ostwald ripening appear to be rather large in comparison to available experimentally observed rates,[44] indicating that these results should be regarded only semiquantitatively (see Supporting Information for a detailed discussion). It should be noted that the experimental data are obtained for larger and more complex molecules than the AM25 studied here; other possible reasons for this discrepancy are discussed further in the Supporting Information. The noise in single measurements is too large to fit this function reliably for the individual traces. This shows that the KJMA law is valid as a description of collective macroscopic quantities of the sample rather than of a single measurement.

Interestingly, during the self-assembly process, we have not observed critical nuclei, i.e., stable clusters of minimal size. We suspected that the absence of stable nuclei is due to the highly dynamic nature of the formed clusters, but (1) the time scale in which the self-assembly is complete may also be too fast for the formation of thermodynamically stable clusters, and (2) the system is relatively small, which may mean that the simulation model still thermodynamically favors well-defined and stable nuclei. We conducted simulations with fewer adsorbent molecules to better sample the early stages of the process and to investigate the intrinsic equilibrium dynamics of the molecules at fixed surface coverages below 90%. Depending on the computational cost of a simulation we performed self-assembly simulations (i.e., starting from randomly distributed molecules in solvent; denoted "SA"), or cheaper rearrangement simulations (i.e., the initial structures already contain molecules adsorbed on the surface, to avoid waiting for adsorbent molecules to reach the surface; denoted "Re"). The results are presented in Figure 3b (blue symbols), which shows the fraction of ordered molecules as a function of bulk concentration at equilibrium. At low concentrations, most of the adsorbent molecules form an unordered phase on the graphite surface. With increasing concentration, at first small (but still dynamic) ordered clusters are observed. Further increased concentration changes the appearance of the system from a liquid phase to an ordered phase, and the number of ordered molecules is increasing. Long-ranged stable domains are only found above ~80% coverage, as evidenced by a high fraction of ordered molecules. Although the fraction of ordered molecules increases with the concentration, we have not observed small stable assemblies, which could act as a nucleus. This behavior was independent of the system size: even if the

DOI: 10.1021/acs.jpcc.9b01234
J. Phys. Chem. C 2019, 123, 17510−17520

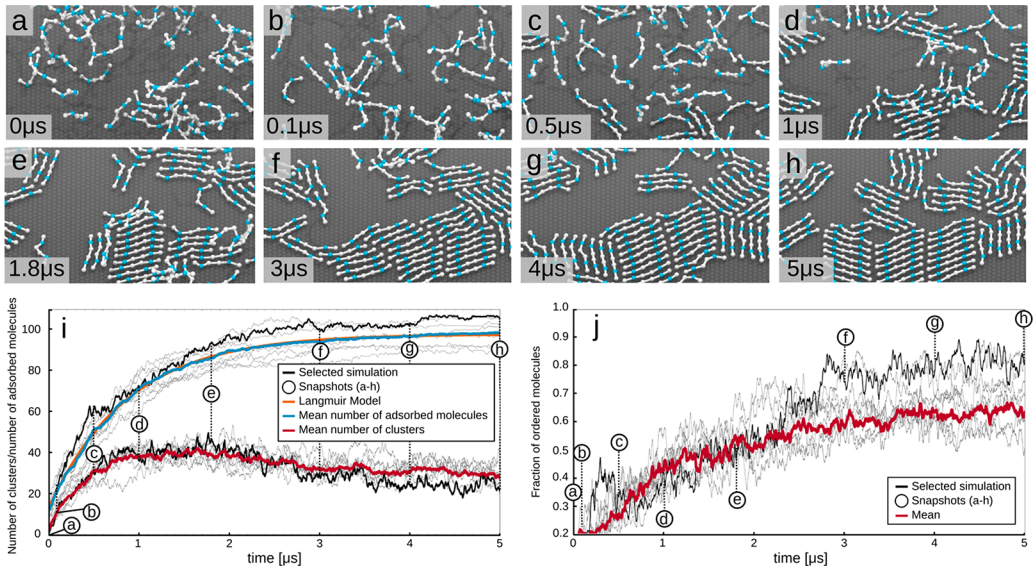

Figure 4. Snapshots from a representative simulation of AM25 at 258 K. (a–h) Adsorption and nucleation phase. (i and j) Information as for Figure 2; see caption to Figure 2.

size of the graphite flake (and the number of adsorbent molecules) was increased by a factor of 4, almost full coverage of the surface was necessary to observe a long-ranged ordered domain (Figure 3b, olive symbols).

Despite the fact that clear nucleation events have not been observed in our simulations, the transition from an unordered to an ordered assembly on the surface can be described using the nucleation-elongation model for 2D self-assemblies at liquid/solid interface, developed by Matsuda et al.[10−15] (Figure 3c). Our modified version of this model (eqs 4 and 5) assumes, that the assembly process can be described by two equilibrium constants: (a) a nucleation constant K_n between an adsorbent molecule in solution or on the surface in an unordered state (denoted A_1^{unord}) and a free surface adsorption site (S) on the one hand and an ordered state (A_1^{ord}) on the other hand (a molecule is in an ordered state when it has two close neighbors with the same orientation, by which we mean it can be parallel or antiparallel; see Supporting Information for details), which acts as a nucleus on the surface; and (b) an elongation constant K_e between an adsorbent molecule in an unordered state and ordered clusters of any size (A_n^{ord}) adsorbed on the surface (note that, in the original model of Matsuda et al.,[13] this equilibrium is only between monomers in solvent and clusters on the surface):

$$A_1^{unord} + S \rightleftarrows A_1^{ord} \text{ with } K_n = \frac{[A_1^{ord}]}{[S][A_1^{unord}]} \tag{4}$$

$$A_n^{ord} + A_1^{unord} \rightleftarrows A_{n+1}^{ord} \text{ with } K_e = \frac{[A_{n+1}^{ord}]}{[A_n^{ord}][A_1^{unord}]} \text{ for } n \geq 1 \tag{5}$$

Using the steady-state approximation, an expression for the surface coverage of ordered molecules, θ, as a function of bulk concentration of adsorbent, c_t, can be derived (a detailed derivation can be found in the Supporting Information):

$$\theta = (1 - \theta)\frac{\sigma K_e(c_t - \alpha\theta)}{\{1 - K_e(c_t - \alpha\theta)\}^2} \tag{6}$$

Here σ is the degree of cooperativity defined as the ratio between the two equilibrium constants for nucleation and elongation, $\sigma = K_n/K_e$, and α is the maximum concentration of ordered molecules on the graphite surface. Parameter σ describes the tendency of formation of ordered structures depending on the number of molecules already present. When σ is close to 1, adsorbed molecules have a high tendency to align with other molecules on the surface, even if just a few molecules are present (referred to in literature as the isodesmic mechanism[13]). When σ is close to 0, this tendency is lower; molecules only tend to order when many molecules are in their vicinity (referred to in literature as the cooperative mechanism[13]). The data obtained for the surface coverage of ordered molecules from the equilibrium simulations at fixed concentration was fitted to the model, using K_e, σ, and α as variables (see Figure 3c). The fit shows that σ is smaller than one, which means that a specific concentration of unordered molecules is needed to be present on the surface before elongation sets in. Indeed, molecules hardly order (i.e., interact only weakly with neighbors) until a certain concentration is reached (see Figure 3c; ordering starts at around $\sim \frac{1}{K_e}$ which corresponds to $c_t \sim 0.04$ M; see also Supporting Information). After this concentration is reached, the system undergoes a phase transition from a liquid-like phase to an ordered phase. Complete ordering of the assembly on graphite starts with bulk concentration above 0.14 M. Since a similar trend can be found for the larger graphite flake, the ordering starts with a specific concentration of molecules on the surface, rather than with a specific number of molecules on the surface (the latter would point to the existence of a critical nucleus of specific size). We also tried to develop a model which explicitly incorporates unordered adsorbed molecules as a separate state; however, the simpler nucleation–elongation model gives the most accurate description of our data (for the other model, see Supporting Information).

An increasingly popular analysis of simulation data is Markov state modeling,[45−47] which has been applied to relatively simple self-assembling systems with some success.[48,49] We investigated two Markov state models (MSMs),

DOI: 10.1021/acs.jpcc.9b01234
J. Phys. Chem. C 2019, 123, 17510−17520

one using the global metrics used thus far to describe the self-assembly process and one using the molecule-based metric that determines which molecules can be classified as neighbors in an ordered cluster. The latter has been advocated as superior in self-assembling systems that form ordered structures.[50] Details can be found in the Supporting Information. Both MSMs indicated similar implied time scales for the slowest processes, suggesting analysis in terms of three hidden states. The three states can be interpreted as one state consisting of largely unordered molecules (free in solution or adsorbed on the surface) and two interconverting states that differ in a subtle manner in their metrics, probably indicating more extensive and less extensive ordered domains. No metastable states are detected in this analysis. A free energy landscape in terms of the global metrics displays only a single minimum, the final assembled, ordered state (see Figure 3d).

Isodesmic Nucleation Mechanism at Low Temperatures. In contrast to the cooperative nucleation observed at higher temperature, we found that at the lower temperature the nucleation mechanism resembles isodesmic nucleation. At high bulk concentration at low temperature, the presence of multiple nuclei in combination with rapid adsorption leads to relatively many domains or defects (particularly zigzag patterns) that do not heal on the time scales simulated here and also does not allow clear distinction of the mechanism (see Supporting Information). Therefore, for simulations at low temperature we used the concentration of AM25 almost twice as low as for the simulation at the higher temperature of 298 K (approximately 0.07 M), to avoid rapid saturation of the surface. In fact, we made sure that the number of adsorbent molecules is insufficient to saturate the surface to be able to better characterize the assembly process. Representative snapshots are shown in Figure 4a−h. In contrast, in simulations for such concentration at higher temperature the final structure does not display any ordering of the assembly as discussed in the previous section (see Figure 3c). At low temperature, randomly distributed molecules in phenyloctane (Figure 4a) adsorb on the surface and quickly aggregate creating small, thermodynamically stable, clusters (Figure 4b,c). These structures act as nucleation sites and grow to larger ordered structures over time as new molecules arrive on the surface and join the existing clusters (Figure 4d−f). It can be seen that the arrival of molecules is slower than at higher temperature, due to slower diffusion in the solution and to lower bulk concentration. The clusters on the surface largely maintain their orientation, and they are not seen to undergo large reorganization on the time scale of the simulation of 5 μs (cf. Figures 4f−h and a movie in the Supporting Information). This is also due to the slower diffusion of molecules and clusters on the surface.

The details of the adsorption and nucleation stages were investigated by running four independent simulations of 5 μs, monitoring the same quantities as at higher temperature and averaging them. The results are shown in Figure 4, parts i and j. In contrast to the self-assembly process at higher temperature, at the lower temperature, right from the start, the number of adsorbed molecules (Figure 4i, blue line) is larger than the number of clusters (Figure 4i, red line), which means that many molecules are part of clusters shortly after they adsorb to the surface. The Langmuir adsorption rate law (a fit is shown as the orange line in Figure 4i) is valid over the length of the simulation. The entire structure consists of many, small, ordered domains at different orientations. This is consistent with experimental evidence showing that, upon surface saturation, the number of domains formed at low temperature is larger than that at high temperature.[51] Mechanisms to heal such defects are discussed elsewhere.[40] At the lower temperature, there is no transition from an unorganized liquid-like phase to a solid phase, and most of the molecules are ordered (Figure 3b). In fitting the nucleation−elongation model (shown in Figure 3c), we assumed that α is the same as for self-assembly at high temperature; i.e., the maximum amount of molecules which can adsorb does not change with temperature. From the fit, it was found that at low temperature σ is close to 1, which confirms that molecules which adsorb on the surface tend to create ordered clusters even for low bulk concentration. Although potentially interesting, MSM was not possible at the lower temperature due to too limited sampling; many more repeats of the simulations and/or adaptive sampling techniques would be required. In closing this section, it should be noted that although at the lower temperature the clusters preserve the overall structure and act as independent and stable nuclei, to some extent they do demonstrate some desorption−adsorption dynamics; i.e., molecules detach from and attach to the clusters during the simulation. More information is given in the Supporting Information.

Similarities to Other Processes. We noticed that processes described here for physisorption are similar to those occurring in crystallization. Two established mechanisms are distinguished for crystal nucleation: the single step nucleation mechanism and the multistep nucleation mechanism.[52,53] In the single step nucleation mechanism, which is based on classical nucleation theory (CNT), molecules strongly interact with each other. Once a critical number of molecules form an assembly, the interactions are holding the molecules together in a stable cluster, called the nucleus. The nucleus grows by acquiring additional molecules, eventually creating a large long-range ordered structure. For our system, a similar mechanism takes place at lower temperature. Molecules strongly interact with each other forming a nucleus (in our case a molecule strongly interacts already with a single neighbor). Alternatively, in the multistep nucleation mechanism, the interaction between molecules is weaker and the system stays in a liquid state: molecules diffuse and interact with each other, but they do not create stable structures. With growing concentration, eventually local oversaturation occurs, in which ordered structure starts to appear, eventually expanding to form long-range ordered structure. This kind of mechanism applies for formation of SAMNs at higher temperature. Molecules first form a liquid-like phase, from which, upon saturation, the ordered structure is formed.

The self-assembly of functionalized alkanes on graphite also resembles the formation of self-assembled monolayers (SAMs) on other surfaces. One of the most studied SAMs systems is thiols on a gold surface. The process can be described as a special form of chemisorption, in which the adsorbent interacts with the substrate by a covalent, but reversible, interaction. The covalent binding and unbinding allows the adsorbent to retain some lateral diffusivity on the gold surface, which is, however, sufficiently slow to make an observation of the processes of adsorption and of rearrangements on the partially covered surface possible by experimental techniques.[54] Similar observations are made here for physisorbed alkane assembly on graphite as described for SAMs: the mechanism is temperature dependent.[54] Below a certain temperature, molecules start to form small ordered domains, which grow and eventually cover

DOI: 10.1021/acs.jpcc.9b01234
J. Phys. Chem. C 2019, 123, 17510−17520

the whole surface. Above this point, molecules do not coalesce and create a condensed phase (liquid-like or ordered structures with lower density). As the concentration of adsorbent on the surface increases, the structure reorganizes into the ordered assembly. Although the underlying nature of the interaction between adsorbent and surface is different, both behaviors are similar, and the most significant difference is their time scale, which in case of the graphite surface is so short that it is challenging to study the process by experimental techniques.

From a molecular simulation perspective, the slowness due to the covalent binding and unbinding equilibrium warrants methods that predict morphology of SAMs by adding molecules one by one, running short steered MD simulations to test if a molecule wants to adsorb to an increasingly occupied surface, as recently done by Dietrich et al.[55] They found that with that procedure, maximum occupation of the surface as known from experiment is not reached in the simulations. The final patterning was therefore later imposed by allowing binding only at certain sites. A better treatment would be to include sampling of the unbinding of the adsorbents, breaking the chemical bonds and possibly full desorption. The technique would need time scales for the slow processes as input. Previous work by us on the physisorbed monolayers revealed that partial desorption of the alkanes is closely linked to the rearrangement of molecules on a saturated surface and that the time scales for these rearrangements are accessible by our model.[40]

CONCLUSION

In this work, we present unprecedented insights concerning the formation of long-range ordered lamellar structures of physisorbed self-assembling long functionalized alkanes on graphite. The simulations show that the overall mechanism consists of two simultaneous processes, being adsorption to and rearrangement on the surface. The rearrangement process starts with nucleation (formation of long-range ordered structures) followed by Ostwald ripening. The mechanism of nucleation is temperature dependent. At lower temperature, the mechanism is more similar to isodesmic nucleation: adsorbed molecules rapidly form independent, small, ordered domains, which subsequently grow by addition of new arrivals. The different orientations of the domains lead to many domain boundaries and the overall order remains low. At higher temperature, the nucleation process can be described by cooperative nucleation. Here, molecules adsorb on the surface forming a liquid-like phase, and only when a certain level of surface coverage by the adsorbent is reached does the whole structure undergoe a phase transition to an ordered structure. In both cases, after the nucleation step, relatively slow corrections of the structure can be described by Ostwald ripening.

Taken together, in this work, we have provided insights into the nucleation mechanism of physisorbed alkanes, which is not accessible by other techniques such as STM. Moreover, our method can be used to predict the structure of the final assembly.

METHODS

Model. A recently developed modified Martini coarse-grained model was used to study the adsorption, structure, and dynamics of functionalized long-chain alkanes on a graphite surface.[33,56] The model treats groups of roughly four atoms (not counting hydrogens) as the basic building blocks, called beads. For aromatic moieties, a two-to-one correspondence (mapping) is used to preserve the ring structure. The mapping of the long-chain functionalized molecules used in this study is shown in Figure 1. The Martini model was originally developed to study the self-assembly, structure, and dynamics of lipids,[57] but was successfully extended to study a variety of other self-assembly processes such as bulk heterojunctions,[58] supramolecular assemblies,[59] and oil−water emulsions.[60] Briefly, bonded interactions include harmonic bonds between neighboring beads and cosine-type harmonic angle potentials between triplets of beads. Nonbonded interactions are modeled using a shifted form of the Lennard-Jones interaction, ensuring that both potential and force smoothly approach zero at the cutoff distance of 1.2 nm, starting the shifting from 0.9 nm. None of the adsorbents used in this study carry partial charges, and there are no Coulomb forces between any of the beads. Beads are classified as hydrophobic (strongly partitioning into alkane solvent over water, C-type) and polar (strongly partitioning into water, P-type). The nonbonded interactions are parametrized based on partitioning free energies between different types of solvent of small model compounds, each represented by a single bead. The modifications of the model to make it suitable for adsorbents on a graphite surface are based on adsorption enthalpies of a range of compounds and on preferential adsorption of long-chain alkanes over short-chain alkanes from a mixed solution. The parametrization involved defining a new bead type for the underlying graphite surface (SG4), optimizing the nonbonded interaction parameters of the beads with the surface and fine-tuning adsorbent−adsorbent interactions, and the bonded parameters describing molecular geometry (bonds, angles, dihedrals), with the aim to semiquantitatively reproduce packing on the surface. The present model uses the alkane (C1S and C1E) and alkanol/amide beads (P1) for the adsorbents and alkane (C1) and aromatic (SC4) beads for the solvent phenyloctane, as described by Gobbo et al.[33] and detailed in the Supporting Information. Validation of the adsorbents is reported in Gobbo et al.;[33] validation of phenyloctane is described in the Supporting Information.

Simulation Details. Simulations were done using the Gromacs package,[61,62] using several installations of versions 4 and 5 on different hardware platforms. The equations of motion were solved numerically using a time-step of 30 fs. A triclinic unit cell (simulation box) was used, with the lateral dimensions (x, y) fixed, so that the basal plane is commensurate with a hexagonal lattice of the graphite beads. The perpendicular dimension (z) was kept orthogonal to the basal plane, but not fixed in length. Periodic boundary conditions were applied in all directions. Pressure coupling to a pressure of 1.0 bar was achieved through the Berendsen barostat[63] with a coupling time of 3.0 ps and a compressibility in the z-direction of 3.0×10^{-5} bar^{-1}. Temperature was maintained by coupling to a bath through a Berendsen thermostat[63] with coupling constant 0.3 ps. Different adsorbents were coupled to separate temperature coupling baths. The graphite beads were always frozen. Thus, there is no dynamics in the beads making up the surface. Simulations were run at 298 and at 258 K. The neighbor list update was done every 10 steps.

Analysis and Visualization. Results were analyzed by MDAnalysis.[64,65] Visualizations have been done by VMD.[66]

DOI: 10.1021/acs.jpcc.9b01234
J. Phys. Chem. C 2019, 123, 17510−17520

Systems. An initial set of simulations was performed with systems consisting of 18 000 graphite beads, 388 adsorbent molecules, and 10 476 phenyloctane molecules, resulting in a bulk concentration of approximately 0.14 M. The graphite surface contains five layers of beads with an area of 227 nm^2 and is a small free-standing flake; i.e., the surface is not connected through periodic boundary conditions. The idea is to avoid possible packing defects of the adsorbents due to imposed periodicity (see Supporting Information). The systems were prepared by first filling the simulation volume with the graphite surface already present with randomly placed adsorbent molecules and subsequently adding randomly placed phenyloctane solvent molecules. The adsorbent molecules were 6-bead and 8-bead linear chains with zero, one, or two polar beads. Representations of the adsorbent molecules are shown in the top panels of Figure 1. In the Martini model, these molecules can be taken as representative of tetracontane ($C_{24}H_{50}$, ALK), tetracosanol ($C_{24}H_{49}OH$, AL1), *N*-heptadecanobutanamide ($C_4H_9-CO-NH-C_{17}H_{35}$, AM2), *N*-tridecanooctanamide ($C_8H_{11}-CO-NH-C_{13}H_{27}$, AM3), *N*,*N*′-decanomethylenebispentamide ($C_4H_9-CO-NH-(CH_2)_{10}-NH-CO-C_4H_9$, AM25), *N*,*N*′-decanomethylenebisnonamide ($C_8H_{17}-CO-NH-(CH_2)_{10}-NH-CO-C_8H_{17}$, AM36), but they may also be interpreted as chains that are one to two atoms longer or shorter and have the amide groups shifted up or down the chain by one or two positions. The adsorbents will be referred to by their polar substituent pattern: ALK, alkane; AL1, alcohol group at bead 1; AM2, amide at bead 2; AM3, amide at bead 3; AM25, amide groups at beads 2 and 5; AM36, amide groups at beads 3 and 6. Except for AM36 which consists of eight beads, all molecules are represented by a six-bead chain. The number of adsorbent molecules in these simulations is such that it allows full coverage of both surfaces by the adsorbent molecules, with some excess molecules remaining in solution. The initial set of simulations was run for at least 10 μs each. It is worth noting that coarse-graining smooths the potential, which results in a speed-up of a process with respect to all-atomistic simulations. For water and lipid systems, the Martini model shows a speed-up of about four times compared to atomistic simulations[56,57] (i.e., 10 μs coarse-grained simulation time is roughly equivalent to 40 μs of all-atom simulation time), but the scaling may be different for the present system and was not investigated. All times reported are coarse-grained simulation times. Simulations for selected systems were repeated with different random starting structures to gather more statistics on the early stages of monolayer formation.

In order to test for nucleation of adsorbent domains on the surface and to study domain size and dynamics at partial surface coverage, additional simulations were performed with a smaller number of adsorbent molecules. For some simulations at 258 K, the initial structures already contain molecules adsorbed on the surface, to avoid simulating the slow process of diffusion of adsorbent molecules unto the surface.

Simulations were also performed on larger systems, multiplying the initial size of the graphite flake by a factor of 4 (2 × 2 in lateral directions) to study formation, organization, and dynamics of larger domains for the molecule showing the most ordered surface structures, AM25. A complete list of simulations is presented in the Supporting Information.

■ ASSOCIATED CONTENT

Supporting Information

The Supporting Information is available free of charge on the ACS Publications website at DOI: 10.1021/acs.jpcc.9b01234.

Additional details about methods including analysis, description of force-field, list of all simulations; details and derivation of nucleation−elongation models; additional results including influence of underlying graphite structure, parametrization and validation of phenyloctane, additional snapshots of final structures, additional analysis of trajectories, details of KJMA fitting, influence of concentration and volume of simulation system, and stability of clusters at lower temperature; and full description of supporting videos and zip files (PDF)

Video of self-assembly of 388 AM25 molecules on graphite surface at 298 K (MPG)

Video of self-assembly of 200 AM25 molecules on graphite surface at 298 K(MPG)

Video of self-assembly of 200 AM25 molecules on graphite surface at 258 K (MPG)

Parameters of the force field used in this work (ZIP)

Short guide for simulation of self-assembly on graphite surface, including the initial setup of the system (ZIP)

■ AUTHOR INFORMATION

Corresponding Author

*(J.H.v.E.) E-mail: j.h.vanesch@tudelft.nl.

ORCID

Siewert J. Marrink: 0000-0001-8423-5277

Steven De Feyter: 0000-0002-0909-9292

Jan H. van Esch: 0000-0001-6116-4808

Notes

The authors declare no competing financial interest.

■ ACKNOWLEDGMENTS

The authors acknowledge the financial support by the EC seventh Framework Programme Marie Curie Actions via the European Initial Training Network SMARTNET No. 316656.

■ REFERENCES

(1) Elemans, J. A. A. W.; Lei, S.; De Feyter, S. Molecular and Supramolecular Networks on Surfaces: From Two-Dimensional Crystal Engineering to Reactivity. *Angew. Chem., Int. Ed.* **2009**, *48* (40), 7298−7333.

(2) Hecht, S. Welding, Organizing, and Planting Organic Molecules on Substrate Surfaces - Promising Approaches towards Nano-architectonics from the Bottom up. *Angew. Chem., Int. Ed.* **2003**, *42* (1), 24−26.

(3) Joachim, C.; Gimzewski, J. K.; Aviram, A. Electronics Using Hybrid-Molecular and Mono-Molecular Devices. *Nature* **2000**, *408* (6812), 541−548.

(4) Kühnle, A. Self-Assembly of Organic Molecules at Metal Surfaces. *Curr. Opin. Colloid Interface Sci.* **2009**, *14* (2), 157−168.

(5) Reed, M. A.; Zhou, C.; Muller, C. J.; Burgin, T. P.; Tour, J. M. Conductance of a Molecular Junction. *Science* **1997**, *278* (5336), 252−254.

(6) Palermo, V.; Samorì, P. Molecular Self-Assembly across Multiple Length Scales. *Angew. Chem., Int. Ed.* **2007**, *46* (24), 4428−4432.

(7) Gutzler, R.; Cardenas, L.; Rosei, F. Kinetics and Thermodynamics in Surface-Confined Molecular Self-Assembly. *Chem. Sci.* **2011**, *2* (12), 2290−2300.

(8) Goronzy, D.; Ebrahimi, M.; Rosei, F.; Arramel; Fang, Y.; Wee, A. T. S.; De Feyter, S.; Tait, S. L.; Wang, C.; Beton, P. H.; et al. Supramolecular Assemblies on Surfaces: Nanopatterning, Functionality, and Reactivity. *ACS Nano* **2018**, *12* (8), 7445−7481.
(9) Barth, J. V.; Costantini, G.; Kern, K. Engineering Atomic and Molecular Nanostructures at Surfaces. *Nature* **2005**, *437* (7059), 671−679.
(10) Yokoyama, S.; Hirose, T.; Matsuda, K. Phototriggered Formation and Disappearance of Surface-Confined Self-Assembly Composed of Photochromic 2-Thienyl-Type Diarylethene: A Cooperative Model at the Liquid/solid Interface. *Chem. Commun.* **2014**, *50* (45), 5964−5966.
(11) Yokoyama, S.; Hirose, T.; Matsuda, K. Effects of Alkyl Chain Length and Hydrogen Bonds on the Cooperative Self-Assembly of 2-Thienyl-Type Diarylethenes at a Liquid/Highly Oriented Pyrolytic Graphite (HOPG) Interface. *Chem. - Eur. J.* **2015**, *21* (39), 13569−13576.
(12) Frath, D.; Sakano, T.; Imaizumi, Y.; Yokoyama, S.; Hirose, T.; Matsuda, K. Diarylethene Self-Assembled Monolayers: Cocrystallization and Mixing-Induced Cooperativity Highlighted by Scanning Tunneling Microscopy at the Liquid/Solid Interface. *Chem. - Eur. J.* **2015**, *21* (32), 11350−11358.
(13) Nishitani, N.; Hirose, T.; Matsuda, K. Investigation on the Surface-Confined Self-Assembly Stabilized by Hydrogen Bonds of Urea and Amide Groups: Quantitative Analysis of Concentration Dependence of Surface Coverage. *Chem. - Asian J.* **2015**, *10* (9), 1926−1931.
(14) Nishitani, N.; Hirose, T.; Matsuda, K. Influence of Multidirectional Interactions on Domain Size and Shape of 2-D Molecular Assemblies. *Langmuir* **2017**, *33* (36), 9151−9159.
(15) Maeda, N.; Hirose, T.; Yokoyama, S.; Matsuda, K. Rational Design of Highly Photoresponsive Surface-Confined Self-Assembly of Diarylethenes: Reversible Three-State Photoswitching at the Liquid/solid Interface. *J. Phys. Chem. C* **2016**, *120* (17), 9317−9325.
(16) Coenen, M. J. J.; Cremers, M.; Den Boer, D.; Van Den Bruele, F. J.; Khoury, T.; Sintic, M.; Crossley, M. J.; Van Enckevort, W. J. P.; Hendriksen, B. L. M.; Elemans, J. A. A. W.; et al. Little Exchange at the Liquid/solid Interface: Defect-Mediated Equilibration of Physisorbed Porphyrin Monolayers. *Chem. Commun.* **2011**, *47* (34), 9666−9668.
(17) Silly, F.; Weber, U. K.; Shaw, A. Q.; Burlakov, V. M.; Castell, M. R.; Briggs, G. A. D.; Pettifor, D. G. Deriving Molecular Bonding from a Macromolecular Self-Assembly Using Kinetic Monte Carlo Simulations. *Phys. Rev. B: Condens. Matter Mater. Phys.* **2008**, *77* (20), 201408.
(18) Weber, U. K.; Burlakov, V. M.; Perdigao, L. M. A.; Fawcett, R. H. J.; Beton, P. H.; Champness, N. R.; Jefferson, J. H.; Briggs, G. A. D.; Pettifor, D. G. Role of Interaction Anisotropy in the Formation and Stability of Molecular Templates. *Phys. Rev. Lett.* **2008**, *100* (15), 156101.
(19) Rohr, C.; Balbas Gambra, M.; Gruber, K.; Constable, E. C.; Frey, E.; Franosch, T.; Hermann, B. A. Molecular Jigsaw: Pattern Diversity Encoded by Elementary Geometrical Features. *Nano Lett.* **2010**, *10* (3), 833−837.
(20) Lei, S.; Tahara, K.; Müllen, K.; Szabelski, P.; Tobe, Y.; De Feyter, S. Mixing Behavior of Alkoxylated Dehydrobenzo [12]-annulenes at the Solid-Liquid Interface: Scanning Tunneling Microscopy and Monte Carlo Simulations. *ACS Nano* **2011**, *5* (5), 4145−4157.
(21) Calmettes, B.; Estrampes, N.; Coudret, C.; Roussel, T. J.; Faraudo, J.; Coratger, R. Observation and Modeling of Conformational Molecular Structures Driving the Self-Assembly of Tri-Adamantyl Benzene on Ag(111). *Phys. Chem. Chem. Phys.* **2016**, *18*, 20281−20289.
(22) Szabelski, P.; De Feyter, S. Chiral Occlusion in Two-Dimensional Binary Supramolecular Networks Studied by the Monte Carlo Method. *CrystEngComm* **2011**, *13*, 5542−5550.
(23) Martsinovich, N.; Troisi, A. Modeling the Self-Assembly of Benzenedicarboxylic Acids Using Monte Carlo and Molecular Dynamics Simulations. *J. Phys. Chem. C* **2010**, *114* (10), 4376−4388.
(24) Chen, J.; Zhu, E.; Liu, J.; Zhang, S.; Lin, Z.; Duan, X.; Heinz, H.; Huang, Y.; De Yoreo, J. J. Building Two-Dimensional Materials One Row at a Time: Avoiding the Nucleation Barrier. *Science* **2018**, *362* (6419), 1135−1139.
(25) Srinivas, G.; Nielsen, S. O.; Moore, P. B.; Klein, M. L. Molecular Dynamics Simulations of Surfactant Self-Organization at a Solid-Liquid Interface. *J. Am. Chem. Soc.* **2006**, *128* (3), 848−853.
(26) Sun, H.; Yang, X. Molecular Simulation of Self-Assembly Structure and Interfacial Interaction for SDBS Adsorption on Graphene. *Colloids Surf., A* **2014**, *462*, 82−89.
(27) Wu, D.; Yang, X. Coarse-Grained Molecular Simulation of Self-Assembly for Nonionic Surfactants on Graphene Nanostructures. *J. Phys. Chem. B* **2012**, *116*, 12048−12056.
(28) Wu, B.; Yang, X. Molecular Simulation of Electrolyte-Induced Interfacial Interaction between SDS/Graphene Assemblies. *J. Phys. Chem. C* **2013**, *117* (44), 23216−23223.
(29) De Feyter, S.; De Schryver, F. C. Two-Dimensional Supramolecular Self-Assembly Probed by Scanning Tunneling Microscopy. *Chem. Soc. Rev.* **2003**, *32* (3), 139−150.
(30) Rabe, J. P.; Buchholz, S. Commensurability and Mobility in Two-Dimensional Molecular Patterns on Graphite. *Science* **1991**, *253* (5018), 424−427.
(31) McGonigal, G. C.; Bernhardt, R. H.; Thomson, D. J. Imaging Alkane Layers at the Liquid/graphite Interface with the Scanning Tunneling Microscope. *Appl. Phys. Lett.* **1990**, *57* (1), 28−30.
(32) De Feyter, S.; Grim, P. C. M.; Van Esch, J. H.; Kellogg, R. M.; Feringa, B. L.; De Schryver, F. C. Nontrivial Differentiation between Two Identical Functionalities within the Same Molecule Studied by STM. *J. Phys. Chem. B* **1998**, *102* (45), 8981−8987.
(33) Gobbo, C.; Beurroies, I.; De Ridder, D.; Eelkema, R.; Marrink, S. J.; De Feyter, S.; Van Esch, J. H.; De Vries, A. H. MARTINI Model for Physisorption of Organic Molecules on Graphite. *J. Phys. Chem. C* **2013**, *117* (30), 15623−15631.
(34) Ciesielski, A.; Palma, C. A.; Bonini, M.; Samori, P. Towards Supramolecular Engineering of Functional Nanomaterials: Pre-Programming Multi-Component 2D Self-Assembly at Solid-Liquid Interfaces. *Adv. Mater.* **2010**, *22* (32), 3506−3520.
(35) Buchholz, S.; Rabe, J. P. Molecular Imaging of Alkanol Monolayers on Graphite. *Angew. Chem., Int. Ed. Engl.* **1992**, *31* (2), 189−191.
(36) Padowitz, D. F.; Sada, D. M.; Kemer, E. L.; Dougan, M. L.; Xue, W. A. Molecular Tracer Dynamics in Crystalline Organic Films at the Solid-Liquid Interface. *J. Phys. Chem. B* **2002**, *106* (3), 593−598.
(37) Lackinger, M.; Griessl, S.; Kampschulte, L.; Jamitzky, F.; Heckl, W. M. Dynamics of Grain Boundaries in Two-Dimensional Hydrogen-Bonded Molecular Networks. *Small* **2005**, *1* (5), 532−539.
(38) Wang, F.; Richards, V. N.; Shields, S. P.; Buhro, W. E. Kinetics and Mechanisms of Aggregative Nanocrystal Growth. *Chem. Mater.* **2014**, *26* (1), 5−21.
(39) Stabel, A.; Heinz, R.; De Schryver, F. C.; Rabe, J. P. Ostwald Ripening of Two-Dimensional Crystals at the Solid-Liquid Interface. *J. Phys. Chem.* **1995**, *99* (2), 505−507.
(40) Piskorz, T. K.; de Vries, A. H.; De Feyter, S.; van Esch, J. H. Mechanism of Ostwald Ripening in 2D Physisorbed Assemblies at Molecular Time and Length Scale by Molecular Dynamics Simulations. *J. Phys. Chem. C* **2018**, *122*, 24380−24385.
(41) Dannenberger, O.; Buck, M.; Grunze, M. Self-Assembly of N-Alkanethiols: A Kinetic Study by Second Harmonic Generation. *J. Phys. Chem. B* **1999**, *103*, 2202−2213.
(42) Schreiber, F. Structure and Growth of Self-Assembling Monolayers. *Prog. Surf. Sci.* **2000**, *65* (5−8), 151−256.
(43) Richards, V. N.; Rath, N. P.; Buhro, W. E. Pathway from a Molecular Precursor to Silver Nanoparticles: The Prominent Role of Aggregative Growth. *Chem. Mater.* **2010**, *22* (11), 3556−3567.

DOI: 10.1021/acs.jpcc.9b01234
J. Phys. Chem. C 2019, 123, 17510−17520

(44) Stabel, A.; Heinz, R.; Rabe, J. P.; Wegner, G.; De Schryver, F. C.; Corens, D.; Dehaen, W.; Sueling, C. STM Investigation of 2D Crystals of Anthrone Derivatives on Graphite: Analysis of Molecular Structure and Dynamics. *J. Phys. Chem.* **1995**, *99* (21), 8690−8697.
(45) Doerr, S.; Harvey, M. J.; Noé, F.; De Fabritiis, G. HTMD: High-Throughput Molecular Dynamics for Molecular Discovery. *J. Chem. Theory Comput.* **2016**, *12* (4), 1845−1852.
(46) Scherer, M. K.; Trendelkamp-Schroer, B.; Paul, F.; Perez-Hernandez, G.; Hoffmann, M.; Plattner, N.; Wehmeyer, C.; Prinz, J. H.; Noe, F. PyEMMA 2: A Software Package for Estimation, Validation, and Analysis of Markov Models. *J. Chem. Theory Comput.* **2015**, *11* (11), 5525−5542.
(47) Husic, B. E.; Pande, V. S. Markov State Models: From an Art to a Science. *J. Am. Chem. Soc.* **2018**, *140*, 2386−2396.
(48) Sengupta, U.; Carballo-Pacheco, M.; Strodel, B. Automated Markov State Models for Molecular Dynamics Simulations of Aggregation and Self-Assembly. *J. Chem. Phys.* **2019**, *150*, 115101.
(49) Perkett, M. R.; Hagan, M. F. Using Markov State Models to Study Self-Assembly. *J. Chem. Phys.* **2014**, *140* (21), 214101.
(50) Mukhtyar, A. J.; Escobedo, F. A. Developing Local Order Parameters for Order − Disorder Transitions From Particles to Block Copolymers : Methodological Framework. *Macromolecules* **2018**, *51*, 9769−9780.
(51) Fang, Y.; Ghijsens, E.; Ivasenko, O.; Cao, H.; Noguchi, A.; Mali, K. S.; Tahara, K.; Tobe, Y.; De Feyter, S. Dynamic Control over Supramolecular Handedness by Selecting Chiral Induction Pathways at the Solution-Solid Interface. *Nat. Chem.* **2016**, *8* (7), 711−717.
(52) Anwar, J.; Zahn, D. Uncovering Molecular Processes in Crystal Nucleation and Growth by Using Molecular Simulation. *Angew. Chem., Int. Ed.* **2011**, *50* (9), 1996−2013.
(53) Davey, R. J.; Schroeder, S. L. M.; Ter Horst, J. H. Nucleation of Organic Crystals - A Molecular Perspective. *Angew. Chem., Int. Ed.* **2013**, *52* (8), 2166−2179.
(54) Schwartz, D. K. Mechanism and Kinetics of Self-Assembled Monolayer Formation. *Annu. Rev. Phys. Chem.* **2001**, *52*, 107−137.
(55) Dietrich, H.; Schmaltz, T.; Halik, M.; Zahn, D. Molecular Dynamics Simulations of Phosphonic Acid-Aluminum Oxide Self-Organization and Their Evolution into Ordered Monolayers. *Phys. Chem. Chem. Phys.* **2017**, *19* (7), 5137−5144.
(56) Marrink, S. J.; Risselada, H. J.; Yefimov, S.; Tieleman, D. P.; de Vries, A. H. The MARTINI Force Field: Coarse Grained Model for Biomolecular Simulations. *J. Phys. Chem. B* **2007**, *111* (27), 7812−7824.
(57) Marrink, S. J.; de Vries, A. H.; Mark, A. E. Coarse Grained Model for Semiquantitative Lipid Simulations. *J. Phys. Chem. B* **2004**, *108* (2), 750−760.
(58) Alessandri, R.; Uusitalo, J. J.; De Vries, A. H.; Havenith, R. W. A.; Marrink, S. J. Bulk Heterojunction Morphologies with Atomistic Resolution from Coarse-Grain Solvent Evaporation Simulations. *J. Am. Chem. Soc.* **2017**, *139* (10), 3697−3705.
(59) Frederix, P. W. J. M.; Patmanidis, I.; Marrink, S. J. Molecular Simulations of Self-Assembling Bio-Inspired Supramolecular Systems and Their Connection to Experiments. *Chem. Soc. Rev.* **2018**, *47* (10), 3470−3489.
(60) Couallier, E.; Riaublanc, A.; David Briand, E.; Rousseau, B. Molecular Simulation of the Water-Triolein-Oleic Acid Mixture: Local Structure and Thermodynamic Properties. *J. Chem. Phys.* **2018**, *148* (18), 184702.
(61) Pronk, S.; Pall, S.; Schulz, R.; Larsson, P.; Bjelkmar, P.; Apostolov, R.; Shirts, M. R.; Smith, J. C.; Kasson, P. M.; Van Der Spoel, D.; et al. GROMACS 4.5: A High-Throughput and Highly Parallel Open Source Molecular Simulation Toolkit. *Bioinformatics* **2013**, *29* (7), 845−854.
(62) Abraham, M. J.; Murtola, T.; Schulz, R.; Pall, S.; Smith, J. C.; Hess, B.; Lindahl, E. Gromacs: High Performance Molecular Simulations through Multi-Level Parallelism from Laptops to Supercomputers. *SoftwareX* **2015**, *1−2*, 19−25.
(63) Berendsen, H. J. C.; Postma, J. P. M.; van Gunsteren, W. F.; DiNola, A.; Haak, J. R. Molecular Dynamics with Coupling to an External Bath. *J. Chem. Phys.* **1984**, *81* (8), 3684−3690.
(64) Gowers, R. J.; Linke, M.; Barnoud, J.; Reddy, T. J. E.; Melo, M. N.; Seyler, S. L.; Domański, J.; Dotson, D. L.; Buchoux, S.; Kenney, I. M.; Beckstein, O. MDAnalysis: A Python Package for the Rapid Analysis of Molecular Dynamics Simulations. *Proceedings of the 15th Python in Science Conference* **2016**, 98−105.
(65) Michaud-Agrawal, N.; Denning, E. J.; Woolf, T. B.; Beckstein, O. MDAnalysis: A Toolkit for the Analysis of Molecular Dynamics Simulations. *J. Comput. Chem.* **2011**, *32* (10), 2319−2327.
(66) Humphrey, W.; Dalke, A.; Schulten, K. VMD: Visual Molecular Dynamics. *J. Mol. Graphics* **1996**, *14* (1), 33−38.
(67) Askadskaya, L.; Rabe, J. P. Anisotropic Molecular Dynamics in the Vicinity of Order-Disorder Transitions in Organic Monolayers. *Phys. Rev. Lett.* **1992**, *69* (9), 1395−1398.
(68) Lim, R.; Li, J.; Li, S. F. Y.; Feng, Z.; Valiyaveettil, S. Formation of Two-Dimensional Supramolecular Chiral Lamellae by Diamide Molecules at the Solution/graphite Interface: A Scanning Tunneling Microscopy Study. *Langmuir* **2000**, *16* (17), 7023−7030.
(69) Zou, B.; Dreger, K.; Mück-Lichtenfeld, C.; Grimme, S.; Schäfer, H. J.; Fuchs, H.; Chi, L. Simple and Complex Lattices of N-Alkyl Fatty Acid Amides on a Highly Oriented Pyrolytic Graphite Surface. *Langmuir* **2005**, *21* (4), 1364−1370.

DOI: 10.1021/acs.jpcc.9b01234
J. Phys. Chem. C 2019, 123, 17510−17520